

# Proportional Power Sharing Control of Distributed Generators in Microgrids

Farzad Aalipour <sup>\*1</sup> and Tuhin Das <sup>†2</sup>

<sup>1,2</sup>University of Central Florida, Department of Mechanical and Aerospace Engineering, Orlando, Florida, 32816

## Abstract

This research addresses distributed proportional power sharing of inverter-based Distributed Generators (DGs) in microgrids under variations in maximum power capacity of DGs. A microgrid can include renewable energy resources such as wind turbines, solar panels, fuel cells, etc. The intermittent nature of such energy resources causes variations in their maximum power capacities. Since DGs in microgrids can be regarded as Multi-Agent-Systems (MASs), a consensus algorithm is designed to have the DGs generate their output power in proportion to their maximum capacities under capacity fluctuations. A change in power capacity of a DG triggers the consensus algorithm which uses a communication map at the cyber layer to estimate the corresponding change. During the transient time of reaching a consensus, the delivered power may not match the load power demand. To eliminate this mismatch, a control law is augmented that consists of a finite-time consensus algorithm embedded within the overarching power sharing consensus algorithm. The effectiveness of the distributed controller is assessed through simulation of a microgrid consisting of a realistic model of inverter-based DGs.

## Keywords

Consensus, Eigenvalue Perturbation, Distributed Control, Finite-Time Consensus, Inverter-based Microgrid, Proportional Power Sharing, Renewable Energy, Transient Control.

## 1 Introduction

Environmentally sustainable electrical energy production depends on renewable energy resources. In this regard, significant amount of researches have been undertaken within the past few decades [1–3]. Conventionally, control of electric power systems and the main power grid was accomplished through a few central controllers. Through emerging renewable energy plants, intelligent loads located in the demand side and computational advances, distributed energy production and management has become viable. DGs as distributed energy production units, together with local loads which are distinct from the main power, is called a microgrid. Microgrids operate in two different operational modes called grid-connected and islanding. A microgrid is said to work in grid-connected mode when it is connected to the main grid via a tie line at the point of common coupling (PCC) where there exists bidirectional power flow from or into the main grid [4]. In contrast, microgrids in islanding mode generates power for local loads [5]. To deploy small-scale DGs

---

\*farzad.aalipour@knights.ucf.edu

†tuhin.das@ucf.edu

including photovoltaic (PV) cells, wind turbines, fuel cells and energy storage systems (ESSs) in microgrids, power electronics inverters are vital interfaces which connect DGs to the power buses [6].

There have been extensive studies conducted on control of inverter-based microgrids during the past decades [7,8]. The control strategies can be classified in different categories including frequency and voltage control or power control [9]. Applying these methods also depends on the microgrid's mode of operation. For instance, in the grid-connected mode the frequency and voltage are imposed by the main grid. However, voltage and frequency control are vital in islanding mode.

In this work, power sharing control of microgrids in grid-connected mode is studied [11]. The problem of power sharing has been studied from the aspect of equal power sharing in [12, 13]. Since DGs possess different capacities, the DGs with higher capacities can share more power than the DGs with lower capacities. The power sharing problem becomes challenging under intermittent nature of power resources. Intermittency causes fluctuations in maximum capacity of DGs, which leads to changes in their output power. Thereby, the total power fluctuates, and the load power may not always be maintained. These fluctuations can be addressed by deploying electrical energy storage (EES) or managing the DGs to flexibly address the variations in their capacities.

Other approaches proposed to address the power sharing problem in microgrids can be categorized either as proportional power sharing [9, 10, 14], or economic dispatch problem (EDP) [15]. The studies [14] and [16] have proposed techniques for proportional power sharing. Here, proportional power sharing is defined as sharing the load among DGs such that each individual DG shares a fraction of the load in proportion to its maximum capacity. A distributed droop control scheme based on nonlinear state feedback proposed in [9] guarantees that DGs share reactive power proportionally. In [32], through a distributed voltage control, the active and reactive power are shared proportionally, for a microgrid with inductive impedance loads. In addition, [33] formulates the proportional power sharing as a tracking problem and solves it for grid-connected spatially concentrated microgrids. However, [9] and [32] study islanding mode, and none of [9, 32, 33] have covered the power mismatch during transient time of their proposed strategies.

On the other hand, EDP is a method to control the power flow among different DGs optimally, where optimality implies minimizing a quadratic performance index assigned to each DG as the cost of their generated power. EDP has been studied through different techniques including the population dynamic method [17], and the lambda iteration [18]. While these methods have been formulated within a centralized control framework, distributed version of EDP can be found in [15, 19].

Motivated by systems with cyber-physical layers, the power sharing control in this study is devised in two layers. The physical layer that consists of DGs, loads, measurement units, etc., is where the power control loop of each DG is established to track the input power command issued from the cyber layer. DGs have their corresponding agents in the cyber layer. Thus, the ideas of MASs can be utilized to establish the DGs' controllers and their interactions. The agents communicate through a communication network in the cyber layer.

The agents can choose different strategies to control the DGs including centralized, decentralized or distributed formats. When the DGs are located in a small region, it is viable to apply centralized controllers. As the number of DGs increases, while geographically scattered in a wide area, applying the centralized controllers faces deficiencies due to some reasons; Firstly, the centralized controller is not reliable due to the dependency of the DGs on a single controller where its malfunctions deteriorate the performance of the microgrid or may result in instability. Besides, in centralized coordinated control, transferring data to a control center and issuing control signals back to DGs require high bandwidth communication, which is not economically efficient, or technically secure, and is prone to failure [20]. On the contrary, distributed control techniques require considerably lower bandwidth which makes the communications among the DGs economically viable. Decentralized controllers are applicable locally, however it does not exploit cooperation of DGs [21]. Therefore, they may not perform efficiently where the global information and cooperation is required. In contrast, a distributed control scheme encompasses the plug and play feature, which it makes

it more flexible compared to centralized and decentralized controllers [22]. The centralized control scheme depends on global information while DGs in distributed control exchange information exclusively with the DGs in their neighborhood. In this study, the well-known consensus algorithm is utilized to design a distributed controller for the power sharing control problem.

Considering a large number of DGs scattered in a wide area, it takes agents time to transfer all the required signals. Therefore, it is inevitable to have communication delays in the distributed controllers [23]. The ranges of these delays are from tens to hundreds of milliseconds [24]. The delays may result in prolonging the convergence time of consensus algorithm and potentially lead to microgrid instability [16]. The delays can be reduced through increasing the convergence rate of consensus algorithms utilizing approaches including multiplying the weights of the communication graph with a large constant, or through an optimization of the weights [25].

This study considers a microgrid operating in grid-connected mode using proportional power sharing. Proportional power sharing makes the microgrid adaptable to intermittency of power sources. The grid-connected operation enables the microgrid to transmit excess power to the main grid, while relying on it for frequency and voltage control. The contributions of this paper are:

- 1) A distributed consensus algorithm is designed, by which the DGs are able to estimate the microgrid's power capacity under perturbations in the power capacity of individual DGs. Convergence rate of the algorithm is studied and bounds on allowable perturbations are derived based on practical constraints.
- 2) Multiple proportional power sharing strategies are proposed, to meet the demanded power as consensus is reached. The strategies are executed in a distributed manner. They ensure that the microgrid satisfies load power variations dynamically and allow excess power to be transmitted to the main grid.
- 3) Items (1) and (2) enable proportional power sharing. However, during convergence of the consensus algorithm, a power mismatch occurs between the generated and demanded power. Although the rate of convergence can be increased, the transient power mismatch remains inevitable. To eliminate this mismatch, a fully distributed finite-time consensus algorithm, based on [27], is additionally augmented.
- 4) A realistic simulation is conducted, using MATLAB's Simscape toolbox, with a clear primary controller scheme and corresponding parameters. Grid and DG parameters used in simulations are also given. The simulations and the results can be reproduced by readers, allowing further enhancements in future research.

The rest of this paper is organized as follows. The preliminary definitions of technical terms are explained in section two. Then, proportional power sharing is defined in the third section. In the fourth section, the consensus algorithm is developed through which the DGs are able to update their information about the total microgrid power capacity following a change in a DG's capacity. The overarching consensus algorithm and the embedded transient controller are proposed and elaborated in the same section. Fifth section discusses the cyber and physical layers which control the output power of DGs. Next, simulation results are provided in section six to illustrate the effectiveness of the proposed control plan in response to different variations in capacity of a DG. Finally, concluding remarks are provided and references are listed.

## 2 Preliminary Definitions

We define the graph  $\mathcal{G}$  as the set pair  $(\mathbf{v}, \mathbf{\varepsilon})$  having vertices set  $\mathbf{v}$  and edge set  $\mathbf{\varepsilon}$ . Let the number of vertices in  $\mathcal{G}$  be  $N$ , and let the set  $\mathbf{\varepsilon}$  consist of the vertices pairs  $(i, j)$  for which there exists an edge that connects  $j$  to  $i$ , with  $i, j = 1, 2, \dots, N$  and  $i \neq j$ . The intended graph in this study is undirected or bidirectional graph, where the signals flow along edges in both directions, i.e. if  $(i, j) \in \mathbf{\varepsilon}$ , then  $(j, i) \in \mathbf{\varepsilon}$ . The adjacency matrix associated with the graph is  $A = [a_{ij}] \in \mathbf{R}^{N \times N}$  where each element  $a_{ij} > 0$  if  $(i, j) \in \mathbf{\varepsilon}$ , otherwise  $a_{ij} = 0$ . As stated above, in the bidirectional graph  $\mathcal{G}$ , if  $(i, j) \in \mathbf{\varepsilon}$ , then  $(j, i) \in \mathbf{\varepsilon}$ , and  $a_{ij} = a_{ji}$ . Then  $A$  is symmetric, i.e.  $A = A^T$ . We define the degree matrix  $D = [d_{ii}] \in \mathbf{R}^{N \times N}$  as a diagonal matrix as such

$$d_{ii} = \sum_{j=1}^N a_{ij} \quad (1)$$

The matrix  $L = [l_{ij}] = D - A$  is denoted as the Laplacian Matrix of  $\mathcal{G}$ . As mentioned above,  $A = A^T$ , and considering  $D$  is a diagonal matrix, it follows that  $L = L^T$ . The neighbor set corresponding to each vertex  $i$  is defined as  $\mathcal{N}_i = \{j | (i, j) \in \varepsilon\}$ . Additionally,  $\mathcal{N}_j^+$  denotes the set of outgoing neighbors of node  $j$ , i.e., the set of nodes receiving signals from the node  $j$ , and  $\mathcal{N}_j^-$  is the set of nodes which sends signals to the node  $j$ . For the bidirectional graph  $\mathcal{G}$ ,  $\mathcal{N}_j^+ = \mathcal{N}_j^-$ . A graph is connected if there exists a path between any two distinct vertices [26]. We assume that  $\mathcal{G}$  is connected.

Next, consider Fig. 1 which shows a sample localized microgrid with four DGs, denoted by  $DG_i$ ,  $i = 1, 2, 3, 4$ . In this figure, the dashed lines show signaling between the cyber layer and physical layer, i.e. the communications between the DGs and their corresponding agents in the cyber layer. The lines with bidirectional arrows represent communications among the corresponding agents of  $DG_i$  located in the cyber layer. The solid lines are electrical connections. Based on the weights shown in Fig. 1 and the explanations above, the adjacency and degree matrices are defined as,

$$A = \begin{bmatrix} 0 & 0 & a_{13} & 0 \\ 0 & 0 & a_{23} & a_{24} \\ a_{31} & a_{32} & 0 & 0 \\ 0 & a_{42} & 0 & 0 \end{bmatrix}, D = \begin{bmatrix} a_{13} & 0 & 0 & 0 \\ 0 & a_{23} + a_{24} & 0 & 0 \\ 0 & 0 & a_{31} + a_{32} & 0 \\ 0 & 0 & 0 & a_{42} \end{bmatrix} \quad (2)$$

Based on the definition of Laplacian matrix, the corresponding Laplacian matrix to the adjacency and diagonal matrices defined in (2) is

$$L = \begin{bmatrix} a_{13} & 0 & -a_{13} & 0 \\ 0 & a_{23} + a_{24} & -a_{23} & -a_{24} \\ -a_{31} & -a_{32} & a_{31} + a_{32} & 0 \\ 0 & -a_{42} & 0 & a_{42} \end{bmatrix} \quad (3)$$

### 3 Problem Definition

We consider a microgrid in the grid-connected mode, where the microgrid's voltage and frequency are imposed by the main grid, i.e. the microgrid's frequency and voltage are fixed. Hence, the goal in this mode is to control the output power of the DGs. The cyber-physical systems considered in this paper is similar to the one shown in Fig. 1. The proposed control emerges from consensus control of Multi-Agent Systems (MAS). The control objective is sharing load power in proportion to the maximum power capacity of the DGs, under variations in maximum capacities. We assume that there exists  $N$  DGs in a microgrid which are labeled as  $DG_i$  where  $i = 1, 2, \dots, N$ . The maximum power capacity and instantaneous output power of each  $DG_i$  are defined as  $P_{i,max}$  and  $P_i$ , respectively. Let  $P_L$  be the load power, which is proportionately shared among the DGs, i.e.

$$P_L = \sum_{i=1}^N P_i, \text{ s.t. } r = \frac{P_1}{P_{1,max}} = \frac{P_2}{P_{2,max}} = \dots = \frac{P_N}{P_{N,max}} \quad (4)$$

where  $r$  is the proportional power share ratio. Thus, the output power of  $DG_i$  is  $P_i = rP_{i,max}$ . Let  $P_T$  be the total power capacity of the microgrid defined as the accumulation of the maximum power capacity of all the DGs in the microgrid. Then, one can conclude that

$$r = \frac{\sum_{i=1}^N P_i}{\sum_{i=1}^N P_{i,max}} = \frac{P_L}{P_T} \quad (5)$$

and the output power of  $DG_i$  is  $P_i = (P_L/P_T) P_{i,max}$ . Note that a fluctuation in the maximum capacity of a DG  $P_{i,max}$  or a change in  $P_L$  will cause a change in  $r$ . The proposed power sharing control will, in response,

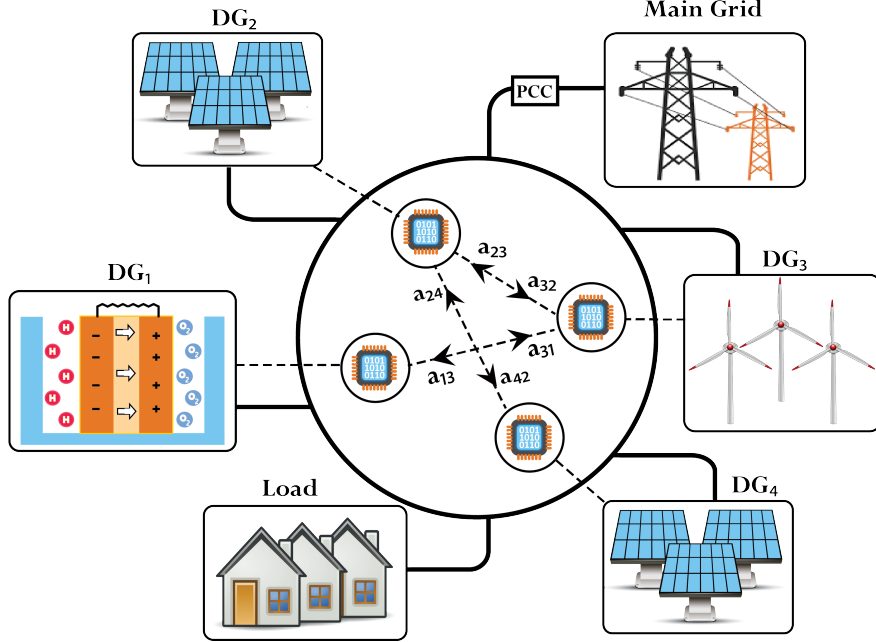


Figure 1: Schematic of a microgrid comprising cyber and physical layers

manage the output power of the DGs flexibly. Throughout this study, the goal is to manage the variations of  $P_i$ s while meeting the requirement  $P_L = \sum_{i=1}^N P_i$ . It is assumed that all DGs have a knowledge of  $P_L$  at all times. The power demand  $P_L$  can vary with time.

We next explain two scenarios for which different controllers are designed. At the core of these controllers is a consensus algorithm which is inherently distributed. Recall that an underlying assumption is that the communication graph among the DGs is connected. Before any change happens to the renewable energy resources, we assume all DGs have the knowledge of  $P_T$  by which they are able to compute  $r$  from (5) and thereby generate their appropriate proportional power share  $P_i = rP_{i,max}$ ,  $i = 1, 2, \dots, N$ .

In the first scenario, assume the maximum capacity of  $DG_k$  which is  $P_{k,max}$ , changes. Then  $P_T$  changes accordingly and all DGs are required to update their value of  $P_T$  to be able to recalculate the new  $r$  based on (5). The only DG that can generate accurate power immediately after a fluctuation happens is the  $DG_k$  since it is aware of the change in  $P_{k,max}$ . Let  $\delta$  be the change such that  $\tilde{P}_{k,max} = P_{k,max} + \delta$ , where  $\tilde{P}_{k,max}$  is the updated value of  $P_{k,max}$ . Thus,  $DG_k$  can compute the updated capacity of the microgrid as  $\tilde{P}_T$  where  $\tilde{P}_T = P_T + \delta$  and recalculate  $r$  and the delivered power  $P_k$ . A consensus algorithm is devised to have other DGs compute the  $\tilde{P}_T$  and thereby reach the new value of  $r$ , distributively.

In the second scenario, we address the mismatch between load and supplied power before consensus is reached. As was discussed in scenario (1), only  $DG_k$  can generate an accurate amount of power instantaneously after a fluctuation in  $DG_k$ . Although the other DGs are able to update  $P_i$  following a change in  $P_{k,max}$ , the consensus algorithm takes time to converge, and hence during the transient time  $\sum_{i=1}^N P_i$  would not necessarily be equal to  $P_L$ . The reason is that the other DGs do not have the correct value of  $\tilde{P}_T$  instantaneously. However, since instantaneous matching of load power is a priority, a control law is augmented with the consensus algorithm to practically remove power mismatch during transients.

## 4 Distributed Microgrid Control

### 4.1 Consensus on Total Power Capacity under Perturbation

We consider a scenario where the individual DGs know the power ratio  $r$  and generate accurate  $P_i$  based on proportional power sharing, as shown in (4). Hence, each DG has correct knowledge of  $P_T$ , as per (5). Next, consider a change in  $P_{k,max}$  to  $\tilde{P}_{k,max} = P_{k,max} + \delta$ . Following this change, all agents are required to compute  $\tilde{P}_T = P_T + \delta$ , the updated value of  $P_T$ . We define  $s_i(t)$  as the estimate of  $\tilde{P}_T$  by DG $_i$ . The vector of estimate variables is then,  $\mathbf{S}(t) = [s_1 \ s_2 \ \cdots \ s_N]^T$ , where  $N$  is the number of the DGs in the microgrid. As mentioned above, all the DGs know  $P_T$  before any change happens. Therefore, the initial value of  $\mathbf{S}$  is,  $\mathbf{S}(0) = P_T \mathbf{1}$  where  $\mathbf{1}^N = [1 \ 1 \ \cdots \ 1]^T$ . Thereafter, we propose the following consensus dynamics in the cyber layer, through which all DGs update their value of  $P_T$  and converge to  $\tilde{P}_T$ .

$$\begin{aligned} \dot{s}_k(t) &= -h(s_k(t) - \tilde{P}_T) - \sum_{j \in \mathcal{N}_k} a_{kj}(s_k(t) - s_j(t)) \\ \dot{s}_i(t) &= -\sum_{j \in \mathcal{N}_i} a_{ij}(s_i(t) - s_j(t)), \quad i = 1, 2, \dots, N, i \neq k \end{aligned} \quad (6)$$

where  $s_k(0) = P_T$  and  $s_i(0) = P_T$ . In (6),  $a_{ij} > 0$  and it denotes the weight of the communication link between agents  $i$  and  $j$ , where  $i, j = 1, 2, \dots, N, i \neq j$ , and  $h > 0$  is a parameter chosen by the  $k^{th}$  agent. The parameter  $h$  represents a measure of the convergence rate of  $s_i(t)$  towards  $\tilde{P}_T$ . Since the communication graph is bidirectional, therefore  $a_{ij} = a_{ji}$ , and this implies that the Laplacian matrix is symmetric, i.e.  $L = L^T$  (see example in (3)). From (6), the following matrix equation is obtained

$$\dot{\mathbf{S}} = -(L + \Delta)\mathbf{S} + hd_k \tilde{P}_T \quad (7)$$

where

$$d_k = \begin{bmatrix} \sigma_{1,k} \\ \sigma_{2,k} \\ \vdots \\ \sigma_{k,k} \\ \vdots \\ \sigma_{N,k} \end{bmatrix} = \begin{bmatrix} 0 \\ 0 \\ \vdots \\ 1 \\ \vdots \\ 0 \end{bmatrix} \in \mathbb{R}^{N \times 1}, \Delta = hd_k d_k^T \in \mathbb{R}^{N \times N} \quad (8)$$

In (8),  $\sigma_{i,k}$  is the *Kronecker Delta* function, implying the  $k^{th}$  element of  $d_k$  is one and rest are zero. Also,  $\Delta_{k,k} = h$  and all other elements are zero. We now propose and prove the following Lemma.

**Lemma 1.** *The linear dynamic system defined in (7) and (8) is input-to-state stable (ISS), and  $S \rightarrow \tilde{P}_T \mathbf{1}$  given the graph of communication among the agents is connected.*

*Proof.* The linear system of (7) and (8) is ISS if  $-(L + \Delta)$  is Hurwitz [28]. The input is  $\tilde{P}_{nom}$  which is constant and bounded, thus, if  $-(L + \Delta)$  is Hurwitz the proof is complete. Since  $L = L^T$ , and by definition  $\Delta = \Delta^T$ , the matrix  $-(L + \Delta)$  is symmetric. Hence, it is Hurwitz if  $-(L + \Delta) < 0$ , i.e. negative definite. To prove this, it is required to show that for any vector  $u \in \mathbb{R}^N$ ,  $u^T [-(L + \Delta)]u$  is strictly less than zero unless  $u = 0$ . From Eq. (8),

$$u^T [-(L + \Delta)]u = -u^T L u - u^T \Delta u = -u^T L u - hu_k^2 \quad (9)$$

where  $h = \Delta_{kk} > 0$ , and  $u_k$  is the  $k^{th}$  element of the vector  $u$ . As the communication graph is connected,  $L$  is positive semi-definite with a single zero eigenvalue [26, 29], and it is diagonalizable [30], with all real eigenvalues. Let  $\lambda_i, i = 1, 2, \dots, N$  be the eigenvalues of  $L$  in descending order,  $\lambda_1 \geq \lambda_2 \geq \dots > \lambda_{N-1} >$

$\lambda_N = 0$ . The canonical form of  $L$  is  $L = V\Lambda V^T$ , where  $\Lambda$  is a diagonal matrix consisting of the eigenvalues of  $L$ , and  $V$  is the right eigenvector-matrix,

$$\Lambda = \begin{bmatrix} \lambda_1 & 0 & & 0 \\ 0 & \lambda_2 & & \\ & & \ddots & \\ 0 & & & \lambda_N \end{bmatrix}, V = [v_1 \ v_2 \ \cdots \ v_N] \quad (10)$$

Since  $v_N$  is the eigenvector corresponding to  $\lambda_N = 0$ , following the definition of  $L$ ,  $v_N = c\mathbf{1}^N$  where  $c \neq 0$  is a real value. Substituting  $L = V\Lambda V^T$  into (9) and taking (10) into account, the following holds:

$$\begin{aligned} -u^T L u - h u_k^2 &= -z^T \begin{bmatrix} \lambda_1 & 0 & & 0 \\ 0 & \lambda_2 & & \\ & & \ddots & \\ 0 & & & \lambda_N \end{bmatrix} z - h u_k^2 \\ &= -\sum_{i=1}^N \lambda_i z_i^2 - h u_k^2 \end{aligned} \quad (11)$$

where  $z = V^T u$ . Since  $V^T$  is a nonsingular matrix it is invertible, and its inverse matrix is  $V$  and  $u = Vz$ . For any  $z = [z_1 \ z_2 \ \cdots \ z_N]^T$  and  $u_k$ , the right hand side of (11) is negative, except  $z_i = 0 \forall i = 1, 2, \dots, N-1$  and  $u_k = 0$ . The remaining condition is  $z = [0 \ \cdots \ 0 \ z_N]^T$ . As  $V$  is not singular,  $u = Vz \neq 0$  while  $z_N \neq 0$ . According to (11) and since  $v_N = c\mathbf{1}^N$ ,

$$u = Vz = [v_1 \ v_2 \ \cdots \ c\mathbf{1}] [0 \ \cdots \ 0 \ z_N]^T = c z_N \mathbf{1} \quad (12)$$

Now that  $u = c z_N \mathbf{1}$  and  $c, z_N \in R$  are non-zero,  $u_k = c z_N \neq 0$ . However, this is in contradiction with the assumption made before which is  $u_k = 0$ . Thus, (11) is negative for any vector  $z$  and since  $u = Vz$ , (9) is negative for any  $u \neq 0$  which proves  $-(L + \Delta)$  is negative definite. We define  $y = \mathbf{S} - \tilde{P}_T \mathbf{1}$ , therefore,  $\mathbf{S} = y + \tilde{P}_T \mathbf{1}$  and  $\dot{\mathbf{S}} = \dot{y}$ . By substituting  $y$  and  $\dot{y}$  into (7), we obtain

$$\dot{y} = -(L + \Delta)y, y = \mathbf{S} - \tilde{P}_T \mathbf{1}, y(t_0) = P_T \mathbf{1} - \tilde{P}_T \mathbf{1} = -\delta \mathbf{1} \quad (13)$$

As  $-(L + \Delta)$  is Hurwitz the dynamics of (13) is exponentially stable. It means  $y \rightarrow 0$  and therefore  $\mathbf{S} \rightarrow \tilde{P}_T \mathbf{1}$ . This completes the proof.  $\square$

We assume that at any time, only one DG can change its power capacity. Thereafter, any subsequent change in power capacity can be done once the consensus algorithm described above has converged.

## 4.2 Observations on Rate of Convergence

From Weyl's theorem on eigenvalue inequalities for sum of two Hermitian matrices [30], the properties of Laplacian matrices in a connected network [29], and Lemma 1, we have

$$\lambda_{N-1}(-L) \leq \lambda_N(-(L + \Delta)) < \lambda_N(-L) = 0$$

assuming the eigenvalues of  $-L$  are ordered as  $\lambda_1(-L) \leq \lambda_2(-L) \leq \cdots \leq \lambda_{N-1}(-L) \leq \lambda_N(-L) = 0$ , and those of  $-(L + \Delta)$  are ordered as  $\lambda_1(-(L + \Delta)) \leq \lambda_2(-(L + \Delta)) \leq \cdots \leq \lambda_{N-1}(-(L + \Delta)) \leq \lambda_N(-(L + \Delta)) < 0$  for all  $h > 0$ . The eigenvalue  $\lambda_N(-(L + \Delta))$  is the dominant eigenvalue of  $-(L + \Delta)$  and hence it determines the rate of convergence of consensus. To explain the effect of  $h$  on convergence rate, we provide the following lemma.

**Lemma 2.** *The rate of convergence of the consensus algorithm, given by (7) and (8), increases with increasing values of  $h > 0$ .*

*Proof.* The characteristic equation of  $-L$  can be expressed as  $p(\lambda) = 0$ . The roots of  $p(\lambda)$ , i.e.  $\lambda_1(-L) \leq \lambda_2(-L) \leq \dots \leq \lambda_{N-1}(-L) \leq \lambda_N(-L) = 0$ , are all real. It can be verified that the characteristic equation of  $-(L + \Delta)$  takes the form  $p(\lambda) + hq(\lambda) = 0$ . Further,  $p(\lambda)$  and  $q(\lambda)$  are both monic polynomials, with  $p(\lambda)$  and  $q(\lambda)$  being polynomials of order  $N$  and  $(N - 1)$  respectively. From Lemma 1, we know that the roots of  $p(\lambda) + hq(\lambda)$  satisfy  $\lambda_1(-(L + \Delta)) \leq \lambda_2(-(L + \Delta)) \leq \dots \leq \lambda_{N-1}(-(L + \Delta)) \leq \lambda_N(-(L + \Delta)) < 0, \forall h > 0$ . Considering the characteristic equation of  $-(L + \Delta)$  in root-locus form, i.e.

$$1 + h \frac{q(\lambda)}{p(\lambda)} = 0, \quad h > 0,$$

we deduce that all roots of  $q(\lambda)$  are real and negative. Otherwise, increasing  $h$  will eventually cause some eigenvalues of  $-(L + \Delta)$  to become complex conjugates and/or unstable, thereby contradicting Lemma 1. This observation is in accordance with the rules of root locus. We further deduce that the largest root of  $q(\lambda)$ , namely  $\lambda_{\max}(q(\lambda))$ , must satisfy

$$\lambda_{N-1}(-L) \leq \lambda_{\max}(q(\lambda)) < \lambda_N(-L) = 0$$

Violating the above condition would also contradict Lemma 1. Since  $\lambda_N(-L) = 0$  and  $\lambda_{\max}(q(\lambda)) < 0$  are the largest roots of  $p(\lambda)$  and  $q(\lambda)$  respectively, there is one branch of root locus that originates from  $\lambda_N(-L)$  and ends at  $\lambda_{\max}(q(\lambda))$  for  $0 \leq h < \infty$ . This branch is also the closest to the origin of all  $N$  branches of the above root locus (which are all strictly along the negative real axis), and hence contains the locus of the dominant eigenvalue of  $-(L + \Delta)$ . With increasing  $h$ , this eigenvalue moves further to the left of the origin, thereby increasing the rate of convergence to the consensus proposed in Lemma 1. This completes the proof.  $\square$

### 4.3 Proportional Power Sharing Strategies

The consensus algorithm of Section 4.1 enable the DGs to compute the updated capacity of the microgrid under perturbation. In this section, we propose methods by which individual agents command power to the physical layer based on consensus. Subsequent to a capacity variation such as  $\delta$  in Section 4.1, three slightly different strategies are proposed through which the DGs meet the load demand  $P_L$ . The first and third strategies are discussed in detail. The second strategy is similar to the first and hence its details are omitted. Assuming at  $t = t_0$ ,  $P_{k,\max}$  changes to  $\tilde{P}_{k,\max} = P_{k,\max} + \delta$ , the first strategy to generate  $P_i$ s is

$$\text{Strategy 1: } \begin{cases} P_k = \frac{P_L}{s_k} \tilde{P}_{k,\max} \\ P_i = \frac{P_L}{s_i} P_{i,\max} \text{ for } i = 1, 2, \dots, N \ i \neq k \end{cases} \quad (14)$$

where  $s_i, i = 1, 2, \dots, N$ , are the estimates of  $\tilde{P}_T$ , as discussed in Section 4.1, and  $\lim_{t \rightarrow \infty} s_i = \tilde{P}_T$  according to Lemma 1. A potential issue may arise when  $s_i(t)$  crosses or approaches zero for some  $t > t_0$  such that  $P_i$  diverges. In this regard, we state and prove the following Lemma:

**Lemma 3.** *Considering the LTI system defined in (7), if  $|\delta| < \theta P_T / (1 + \sqrt{N})$  with  $0 < \theta < 1 - (P_L / P_T)$ , the following holds*

$$(1 - \theta)P_T \leq s_i(t) \leq (1 + \theta)P_T, \quad P_i(t) < P_{i,\max}, \quad \forall t > t_0 \quad (15)$$



The proof of Lemma 3 is given in the Appendix. From Lemma 3, it may appear that as the number of DGs,  $N$ , increases, there will be a bigger restriction on  $\delta$ , since  $|\delta| < \theta P_T / (1 + \sqrt{N})$ . However, it can be shown that the above inequality is not restrictive, mainly because as  $N$  increases,  $P_T$  also increases. An analysis of this aspect is given in the Appendix. From Lemma 3, it may also appear that the constraint on  $\delta$  is restrictive as  $\theta \rightarrow 0$ , which happens as  $P_L \rightarrow P_T$ . This restriction is however justified, since  $P_L \approx P_T$  practically implies that the grid is already close to maximum capacity. Hence, further perturbation in DGs may prevent it from meeting the load demand. So far, it is proved that strategy 1 is valid provided changes in  $\delta$  satisfy the conditions in Lemma 3. Defining the total instantaneous output power of the microgrid as  $P_O(t)$ , from (14),

$$P_O(t) = \frac{P_L}{s_k} \tilde{P}_{k,max} + \sum_{i=1, i \neq k}^N \frac{P_L}{s_i} P_{i,max} \quad (16)$$

Therefore,

$$P_O(t) = \frac{P_L}{s_k} \delta + \sum_{i=1}^N \frac{P_L}{s_i} P_{i,max} \quad (17)$$

Thus, defining the instantaneous error  $E(t) = P_O(t) - P_L$ , we have,

$$E(t) = P_O(t) - P_L = \frac{P_L}{s_k} \delta + \sum_{i=1}^N \frac{P_L}{s_i} P_{i,max} - P_L \quad (18)$$

At  $t = t_0$ ,  $s_i = P_T$  for  $i = 1, 2, \dots, N$ . Thus,

$$E(t_0) = P_L \left[ \frac{\delta}{P_T} + \sum_{i=1}^N \frac{P_{i,max}}{P_T} - 1 \right] \quad (19)$$

Since  $\sum_{i=1}^N \frac{P_{i,max}}{P_T} = 1$ , therefore

$$E(t_0) = P_L \frac{\delta}{P_T} \quad (20)$$

Equation (20) shows that  $E(t_0) \neq 0$ , and since  $E(t)$  is continuous, it implies that a perturbation  $\delta$  causes a transient mismatch between the delivered power  $P_O(t)$  and the load  $P_L$ . The error  $E(t) \rightarrow 0$  at steady-state, as proven in Lemma 1. Therefore, Strategy 1 given in (14), causes a temporary mismatch of power following a perturbation. This issue is addressed in Section 4.4.

The second strategy, which is slightly different from the first one, is as follows:

$$\text{Strategy 2: } \begin{cases} P_k = \frac{P_L}{\tilde{P}_T} \tilde{P}_{k,max} \\ P_i = \frac{P_L}{s_i} P_{i,max} \text{ for } i = 1, 2, \dots, N \text{ } i \neq k \end{cases} \quad (21)$$

As before, the total instantaneous output power of the microgrid  $P_O(t)$  is

$$P_O(t) = \frac{P_L}{P_T + \delta} (\tilde{P}_{k,max}) + \sum_{i=1, i \neq k}^N \frac{P_L}{s_i} P_{i,max} \quad (22)$$

We again evaluate the error  $E(t) = P_O(t) - P_L$  for  $t \geq t_0$ , yielding

$$E(t) = \frac{P_L}{P_T + \delta} (P_{k,max} + \delta) + \sum_{i=1, i \neq k}^N \frac{P_L}{s_i} P_{i,max} - P_L \quad (23)$$

Upon simplifying, we obtain

$$E(t) = P_L \left[ \frac{(P_{k,max} + \delta)}{P_T + \delta} + \sum_{i=1, i \neq k}^N \frac{P_{i,max}}{s_i} - 1 \right]$$

Since at  $t = t_0$ ,  $s_i = P_T$  for  $i = 1, 2, \dots, N$ , and  $\sum_{i=1, i \neq k}^N P_{i,max} = P_T - P_{k,max}$ ,

$$E(t_0) = P_L \frac{\delta(P_T - P_{k,max})}{P_T(P_T + \delta)} \quad (24)$$

Equation (24) shows that  $E(t_0) \neq 0$ , and since  $E(t)$  is continuous, it implies that similar to Strategy 1, a perturbation  $\delta$  causes a transient mismatch between the delivered power  $P_O(t)$  and the load  $P_L$  in Strategy 2. The error  $E(t) \rightarrow 0$  at steady-state, as proven in Lemma 1.

The last candidate strategy is proposed as

$$\text{Strategy 3: } \begin{cases} P_k = \frac{P_L}{s_k} (P_{k,max} + s_k - P_T) \\ P_i = \frac{P_L}{s_i} P_{i,max} \text{ for } i = 1, 2, \dots, N, i \neq k \end{cases} \quad (25)$$

The Strategy 3 allows DGs to update their output power more smoothly compared to the first two strategies. In this case,

$$P_O(t) = \frac{P_L}{s_k} (P_{k,max} + s_k - P_T) + \sum_{i=1, i \neq k}^N \frac{P_L}{s_i} P_{i,max} \quad (26)$$

Therefore,

$$E(t) = P_L \left[ -\frac{P_T}{s_k} + \sum_{i=1}^N \frac{P_{i,max}}{s_i} \right] \quad (27)$$

Since  $s_i = P_T$  for all  $i = 1, 2, \dots, N$ , at  $t = t_0$ ,  $E(t_0) = 0$ . However,  $E(t)$  still undergoes transient fluctuations. Based on (27),

$$\frac{\dot{E}(t)}{P_L} = \frac{P_T \dot{s}_k(t)}{s_k^2(t)} - \sum_{i=1}^N \frac{P_{i,max} \dot{s}_i(t)}{s_i^2(t)} \quad (28)$$

Equation (28) can be further simplified using (7) as follows,

$$\begin{aligned} \frac{\dot{E}(t)}{P_L} &= \frac{P_T \dot{s}_k}{s_k^2} - \\ &\left[ \frac{P_{1,max}}{s_1^2} \quad \frac{P_{2,max}}{s_2^2} \quad \dots \quad \frac{P_{N,max}}{s_N^2} \right] \\ &\times [-(L + \Delta)S + hd_k(P_T + \delta)] \end{aligned} \quad (29)$$

Since at  $t = t_0$ ,  $s_i = P_T$  for all  $i = 1, 2, \dots, N$ ,  $\mathbf{S}(t_0) = P_T \mathbf{1}$  and (29) becomes

$$\begin{aligned} \frac{\dot{E}(t_0)}{P_L} &= \frac{P_T \dot{s}_k(t_0)}{P_T^2} - \\ &\left[ \frac{P_{1,max}}{P_T^2} \quad \frac{P_{2,max}}{P_T^2} \quad \dots \quad \frac{P_{N,max}}{P_T^2} \right] \\ &\times [-L\mathbf{1}P_T - hd_k P_T + hd_k P_T + hd_k \delta] \end{aligned} \quad (30)$$

Simplifying (30) yields

$$\frac{\dot{E}(t_0)}{P_L} = \frac{P_T \dot{s}_k(t_0)}{P_T^2} - \frac{hP_{k,max} \delta}{P_T^2} \quad (31)$$

Referring to (7), at  $t = t_0$ , the term  $\dot{s}_k(t_0)$  in (31) is

$$\dot{s}_k(t_0) = h(P_T + \delta) - hP_T = h\delta \quad (32)$$

Therefore, from (31) and (32),

$$\frac{\dot{E}(t_0)}{P_L} = h\delta \frac{P_T - P_{k,max}}{P_T^2} \quad (33)$$

where from (6),  $h$  is a positive scalar chosen by  $k^{th}$  agent. Thus, although  $E(t_0) = 0$ ,  $\dot{E}(t_0) \neq 0$ . Therefore, as  $E(t)$  is continuous, similar to Strategies 1 and 2, a change  $\delta$  results in a transient mismatch between  $P_O$  and  $P_L$ . It is shown that the three strategies proposed above match the load power  $P_L$  at steady-state while producing transient deviations. This transient issue is resolved in the next section, where a strategy is proposed to practically maintain  $P_O = P_L$  at any time.

#### 4.4 Proportional Power Sharing with Transient Power Match

Upon a perturbation in  $P_{k,max}$ , which results in a change in  $P_T$ , the agents estimate  $\tilde{P}_T = P_T + \delta$  through (7). Among the DGs, only  $DG_k$  has a knowledge of  $\tilde{P}_T = P_T + \delta$ . The other DGs in the microgrid converge to  $\tilde{P}_T$  through consensus only at steady-state. This leads to the transient power mismatch discussed in Section 4.3. To remove this transient mismatch, we propose a strategy where  $DG_k$  modulates its power delivery as follows, while the other DGs maintain the same strategy as in Section 4.3:

$$\begin{aligned} P_k &= \frac{P_L}{s_k} P'_{k,max} \\ P_i &= \frac{P_L}{s_i} P_{i,max} \quad \text{for } i = 1, 2, \dots, N \quad i \neq k \end{aligned} \quad (34)$$

where  $P'_{k,max}$  is an auxiliary dynamic variable required to modulate the instantaneous power of  $DG_k$ . Hence, at  $t = t_0$ ,  $P'_{k,max}(t_0) = P_{k,max}(t_0)$ , and it is required to converge to  $(P_{k,max} + \delta)$  while  $s_i$  converges via consensus. With the goal of maintaining  $P_O(t) = P_L$  for all  $t > t_0$ , we must have

$$P_L = P_O(t) = \frac{P_L}{s_k} P'_{k,max} + \sum_{i=1, i \neq k}^N \frac{P_L}{s_i} P_{i,max} \quad (35)$$

Thus,

$$\frac{P'_{k,max}}{s_k} + \sum_{i=1, i \neq k}^N \frac{P_{i,max}}{s_i} - 1 = 0 \quad (36)$$

Therefore,  $P'_{k,max}$  is

$$P'_{k,max}(t) = s_k(t) \left[ 1 - \sum_{i=1, i \neq k}^N \frac{P_{i,max}}{s_i(t)} \right] \quad (37)$$

The algorithm for updating  $P'_{k,max}$  and  $s_i$  for  $i = 1, 2, \dots, N$  in (34) is as follows:

$$P'_{k,max}(t) = s_k(t) \left[ 1 - \sum_{i=1, i \neq k}^N \frac{P_{i,max}}{s_i(t)} \right] \quad (38a)$$

$$\dot{\mathbf{S}} = -(L + \Delta)\mathbf{S} + hd_k \tilde{P}_T \quad \text{where } \mathbf{S}(t_0) = P_T \mathbf{1} \quad (38b)$$

Based on (34) and (38), we state and prove the following lemma:

**Lemma 4.** *The dynamic system of (38) is stable, i.e. the terms  $P'_{k,max}$ ,  $\frac{P_{i,max}}{s_i}$  and  $\mathbf{S}$  remain bounded if  $|\delta| < \theta P_T / (1 + \sqrt{N})$ , where  $0 < \theta < 1 - (P_L/P_T)$ . Furthermore,  $P'_{k,max} \rightarrow \tilde{P}_{k,max}$  and  $\mathbf{S} \rightarrow \tilde{P}_T \mathbf{1}$ , while the instantaneous delivered power satisfies (35) for all  $t \geq t_0$ .*

*Proof.* Since (38b) is equivalent to (7), per Lemma 1, the dynamic system of (38b) is ISS. Therefore  $\mathbf{S}$  is bounded. Additionally, as (38b) and (7) have the same initial conditions, i.e.  $\mathbf{S}(t_0) = P_T \mathbf{1}$ , thus  $\mathbf{S} \rightarrow \tilde{P}_T \mathbf{1}$ . Following  $|\delta| < \theta P_T / (1 + \sqrt{N})$ , from Lemma 3 we have  $(1 - \theta)P_T \leq s_i(t) \leq (1 + \theta)P_T$  with  $0 < \theta < 1 - (P_L/P_T)$ . Thus,

$$\frac{P_{i,max}}{(1 + \theta)P_T} \leq \frac{P_{i,max}}{s_i} \leq \frac{P_{i,max}}{(1 - \theta)P_T} \quad (39)$$

Therefore,  $\frac{P_{i,max}}{s_i}$  is bounded for all  $i = 1, 2, \dots, N$ . It demonstrates that (38a) represents a viable way to update  $P'_{k,max}$ . By plugging  $P'_{k,max}$  from (38a) into (34),  $P_O(t)$  simplifies to

$$P_O(t) = \frac{P_L}{s_k} s_k \left[ 1 - \sum_{i=1, i \neq k}^N \frac{P_{i,max}}{s_i} \right] + \sum_{i=1, i \neq k}^N \frac{P_L}{s_i} P_{i,max} = P_L \quad (40)$$

for all  $t \geq t_0$ . Since  $\mathbf{S}$  converges to  $\tilde{P}_T \mathbf{1}$ , from (38a) we therefore deduce

$$P'_{k,max}(t) \rightarrow \tilde{P}_T \left[ 1 - \sum_{i=1, i \neq k}^N \frac{P_{i,max}}{\tilde{P}_T} \right] = \tilde{P}_{k,max} \quad (41)$$

This completes the proof.  $\square$

The controller designed in (38a) and (38b) maintains  $P_O(t) = P_L$  following a variation in the power capacity of a DG, namely  $P_{k,max}$ . However, to compute the term

$$\sum_{i=1, i \neq k}^N \frac{P_{i,max}}{s_i} \quad (42)$$

in  $P'_{k,max}$ , as given in (38a), the  $k^{th}$  agent requires additional information. The following approach is proposed to enable the  $k^{th}$  agent to attain this information distributively. This approach is based on the distributed finite-time average consensus studied in [27]. According to [27], each agent  $i$ , shares  $\frac{P_{i,max}}{s_i(t)}$  to its outgoing neighbors  $\mathcal{N}_i^+$  where, following Section 2,  $\mathcal{N}_i^+$  stands for the set of nodes which receives signals from node  $i$ . Accordingly, based on what follows the agents are able to distributively compute the instantaneous average of all  $\frac{P_{i,max}}{s_i(t)}$  where  $i = 1, 2, \dots, N$ , i.e.

$$C_a(t) = \frac{\sum_{i=1}^N \frac{P_{i,max}}{s_i(t)}}{N} \quad (43)$$

Then, the  $k^{th}$  agent can compute (42) via

$$\sum_{i=1, i \neq k}^N \frac{P_{i,max}}{s_i} = N C_a(t) - \frac{P_{k,max}}{s_k} \quad (44)$$

One example of applying this distributed finite-time average consensus is presented in [31]. Similar to [31], the steps of executing the finite-time algorithm is as following:

$$\begin{aligned} \bar{g}_i(m+1) &= p_{ii} \bar{g}_i(m) + \sum_{j \in \mathcal{N}_i^-} p_{ij} \bar{g}_j(m) \\ g_i(m+1) &= p_{ii} g_i(m) + \sum_{j \in \mathcal{N}_i^-} p_{ij} g_j(m) \end{aligned} \quad (45)$$

where  $\bar{g}_i(0) = \frac{P_{i,max}}{s_i}$  and  $g_i(0) = 1$  for  $i = 1, 2, \dots, N$ . Additionally,  $p_{ij} = \frac{1}{1+|\mathcal{N}_j^+|}$  for  $i \in \mathcal{N}_j^+ \cup \{j\}$ , otherwise is zero. Let us define the vectors

$$\begin{aligned}\bar{g}_{i,2m}^T &= [\bar{g}_i(1) - \bar{g}_i(0), \bar{g}_i(2) - \bar{g}_i(1), \dots, \bar{g}_i(2m+1) - \bar{g}_i(2m)] \\ g_{i,2m}^T &= [g_i(1) - g_i(0), g_i(2) - g_i(1), \dots, g_i(2m+1) - g_i(2m)]\end{aligned}\quad (46)$$

and the following Hankel matrices

$$\Gamma\{\bar{g}_{i,2m}^T\} \triangleq \begin{bmatrix} \bar{g}_{i,2m}(1) & \cdots & \bar{g}_{i,2m}(m+1) \\ \bar{g}_{i,2m}(2) & \cdots & \bar{g}_{i,2m}(m+2) \\ \vdots & \ddots & \vdots \\ \bar{g}_{i,2m}(m+1) & \cdots & \bar{g}_{i,2m}(2m+1) \end{bmatrix}\quad (47)$$

and

$$\Gamma\{g_{i,2m}^T\} \triangleq \begin{bmatrix} g_{i,2m}(1) & \cdots & g_{i,2m}(m+1) \\ g_{i,2m}(2) & \cdots & g_{i,2m}(m+2) \\ \vdots & \ddots & \vdots \\ g_{i,2m}(m+1) & \cdots & g_{i,2m}(2m+1) \end{bmatrix}\quad (48)$$

Each agent  $i$  runs the steps in (45) for  $2N+1$  times and keeps the values  $\bar{g}_i(m)$  and  $g_i(m)$  for  $m = 1, 2, \dots, 2N+1$ . Having  $\bar{g}_i(m)$  stored for the  $2N+1$ , each agent  $i$  establishes the vectors  $\bar{g}_{i,2m}^T$  and  $g_{i,2m}^T$  defined in (46) starting from  $m = 0$ . At the same time, all individual agents construct their Hankel matrices  $\Gamma\{\bar{g}_{i,2m}^T\}$  and  $\Gamma\{g_{i,2m}^T\}$  defined in (47) and (48), respectively. Additionally, they calculate the ranks of the Hankel matrices for each  $m$  and repeat the same procedure for the next  $m+1$  until for a specific  $m$  either  $\Gamma\{\bar{g}_{i,2m}^T\}$  or  $\Gamma\{g_{i,2m}^T\}$  becomes a defective matrix. Assume  $\Gamma\{\bar{g}_{i,2M_i}^T\}$  or  $\Gamma\{g_{i,2M_i}^T\}$  is the first matrix which loses its full rank where  $\beta_i = [\beta_{i,0}, \dots, \beta_{i,M_i-1}, 1]^T$  is its corresponding kernel. Having the kernel  $\beta_i$ , the  $i^{th}$  agent computes the average of all  $\bar{g}_i(0) = \frac{P_{i,max}}{s_i}$  for  $i = 1, 2, \dots, N$  defined as  $C_a$  in (43) through the following

$$C_a(t) = \frac{1}{N} \sum_{i=1}^N \bar{g}_i(0) = \frac{[\bar{g}_i(0), \bar{g}_i(1), \dots, \bar{g}_i(M_i)] \beta_i}{[g_i(0), g_i(1), \dots, g_i(M_i)] \beta_i}\quad (49)$$

Thereby, the  $k^{th}$  agent achieves  $C_a(t)$ , distributively. At this step, the  $k^{th}$  agent obtains the term in (42) via (44). By plugging (42) back to (37) the  $k^{th}$  agent is able to compute  $P'_{k,max}$ .

To implement the proposed strategy practically, the mentioned procedures are required to be discretized firstly, since in practice the signals and algorithms update, digitally. We define an index  $w$ , starting from  $w = 0$ , that represents the discrete instants at which the overall consensus algorithm is executed. At  $w = 0$ , the  $i^{th}$  agent,  $i = 1, 2, \dots, N$ , has the value of  $s_i(w) = P_T$ . Therefore, they can compute  $P_{i,max}/s_i(w)$ , individually. Following the finite-time algorithm, they implement the procedure in (45)-(49). Now that all the agents, including the  $k^{th}$  agent, obtains  $C_a(w)$  from (49), then using  $C_a(w)$ , the  $k^{th}$  agent computes

$$P'_{k,max}(w) = s_k(w) \left[ 1 - \sum_{i=1, i \neq k}^N \frac{P_{i,max}}{s_i(w)} \right]\quad (50)$$

The command signals to DGs are as follows

$$\begin{aligned}P_k(w) &= \frac{P_L(w)}{s_k(w)} P'_{k,max}(w) \\ P_i(w) &= \frac{P_L(w)}{s_i(w)} P_{i,max} \quad \text{for } i = 1, 2, \dots, N \quad i \neq k\end{aligned}\quad (51)$$

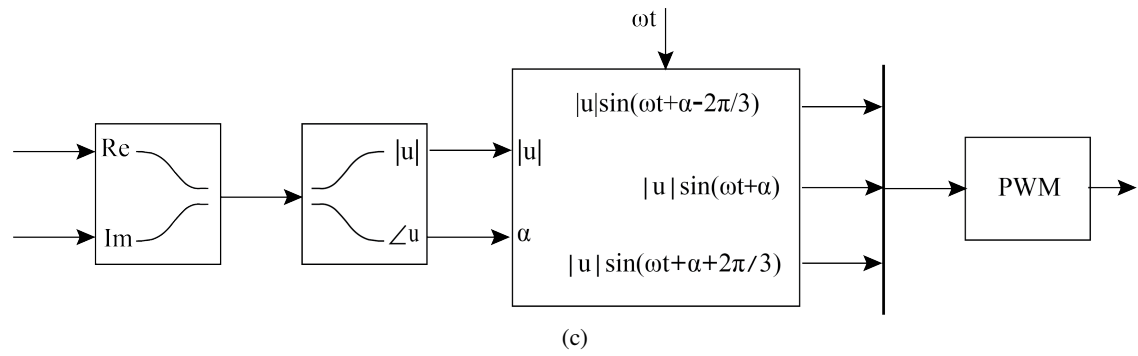
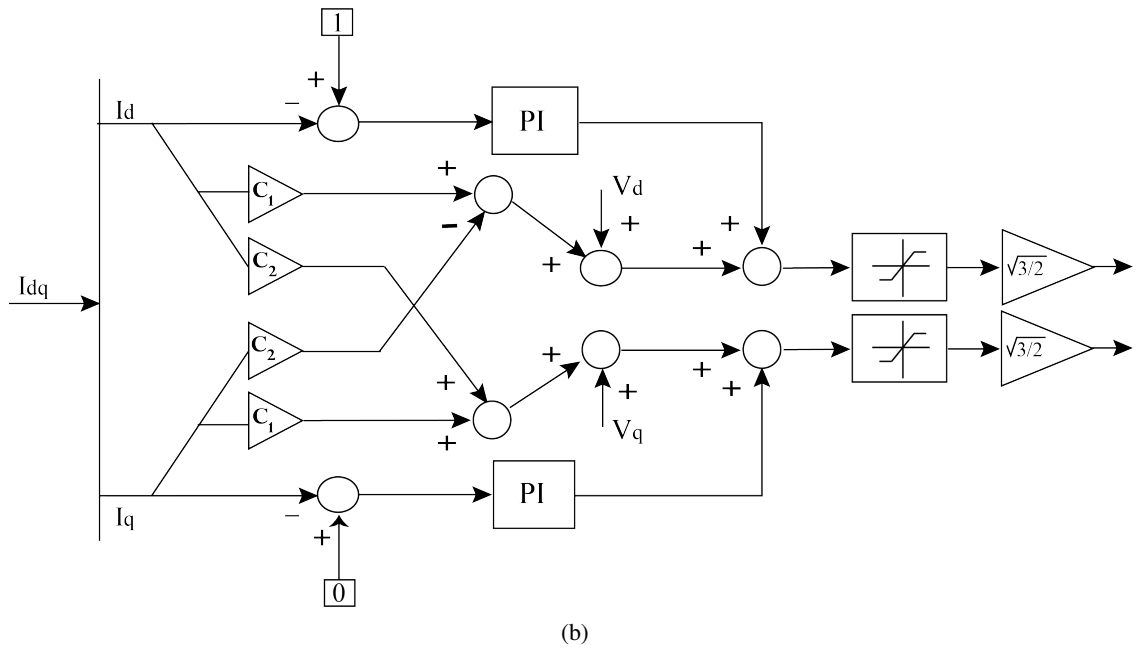
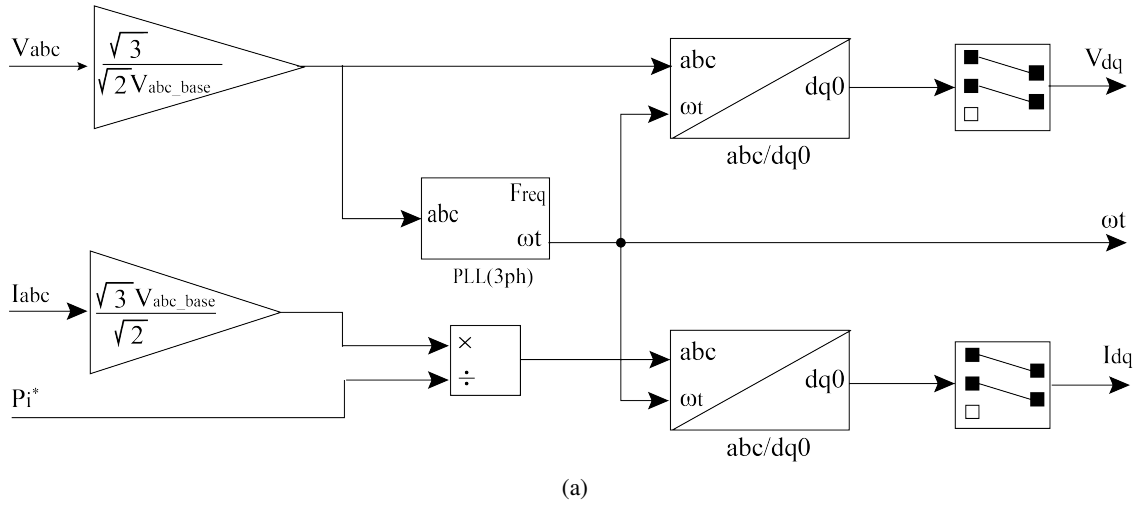


Figure 2: Physical layer control scheme

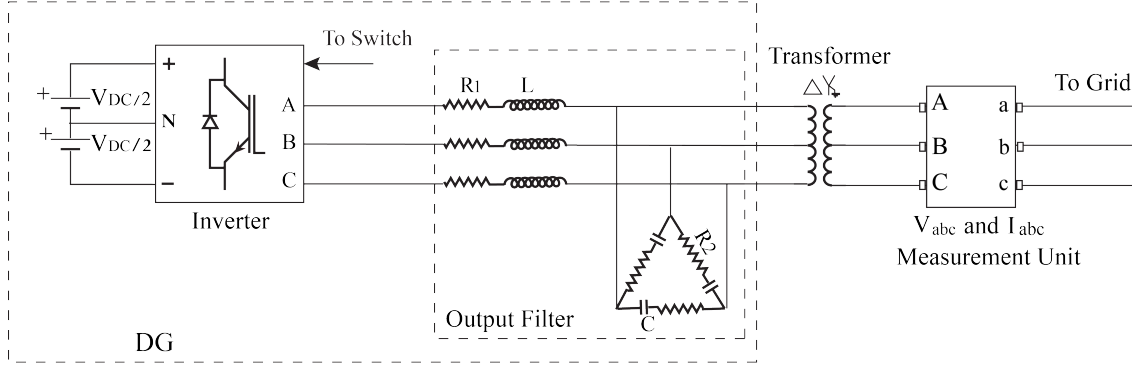


Figure 3: Power circuit diagram of a DG

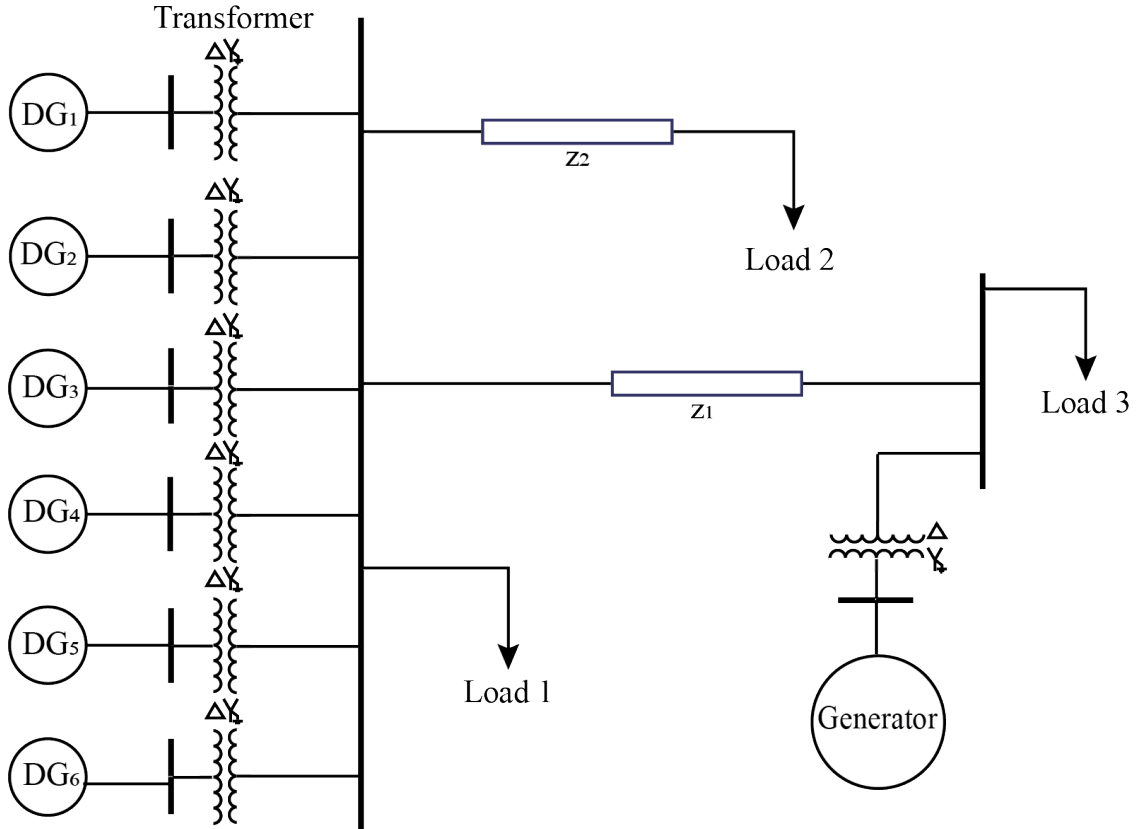


Figure 4: Simulated microgrid bus system

Thereafter, the agents compute  $s_i(w+1)$  through

$$\mathbf{S}(w+1) = \mathbf{S}(w) + dt[-(L + \Delta)\mathbf{S}(w) + hd_k \tilde{P}_T] \quad (52)$$

Set  $w = w+1$ , and repeat the above strategy with the updated value of the  $s_i(w)$  defined in (52). We end this section with the following two observations:

**Remark 1.** The consensus algorithms proposed are independent from the load demand  $P_L$  and its changes, referring to 4.1 and 4.4.

**Remark 2.** All agents in the cyber layer have access to the instantaneous value of  $P_L$ . The power generation

command for strategies 1, 2 and 3 introduced in 4.3 and the control scheme in 4.4 incorporate  $P_L$  and  $s_i(t)$  in the commanded power. Therefore, during consensus the power demand is met, irrespective of whether  $P_L$  changes or not.

## 5 Controller Layout of Physical Layer

The proposed power control methods for DGs introduced in this study are required to be implemented on both cyber and physical layer of microgrids. The physical layer which includes DGs is where controllers are designed to control the output power of DGs. In this study, the problem of proportional power sharing is addressed in the grid-connected mode, hence the frequency and voltage of DGs are imposed by the main grid. Therefore, frequency and voltage control methods, such as droop control, are not considered in this study. Furthermore, the reactive power control in the grid-connected mode is not studied for the practical reason of availability of reactive power in the main grid. Therefore, the required reactive power of the microgrid can be maintained from the main grid.

The desired active power command of each  $DG_i$ , i.e.  $P_i^*$  for  $i = 1, 2, \dots, N$  is calculated by its corresponding agent, i.e.  $i^{th}$  agent in the cyber layer. Then, this signal of  $P_i^*$  is sent to the power control block of  $DG_i$  located in the physical layer. The power control block of DGs is represented in Fig. 2a. This block receives the voltage  $V_{abc}$  and current  $I_{abc}$  from the voltage and current measurement units installed on the output of each DG, as shown in Fig. 3. Figure 3 also shows that each DG is connected to the main grid via a dedicated transformer to match the voltage between the DG and the main grid, as the output voltage of the main grid is significantly higher than the output voltage of DGs. To control the generated power of a  $DG_i$ , i.e.  $P_i$ , it is required to control its output current since  $V_{abc}$  and the frequency of the microgrid are fixed by the main grid. To achieve this, the desired active power command  $P_i^*$  issued from  $i^{th}$  agent is also considered as the other input in Fig. 2a. Using the Phase-Locked-Loop (PLL) block, the signals in Fig. 2a are converted to their equivalent values in the  $dq0$  reference frame, i.e.  $V_{dq}$  and  $I_{dq}$ .

Next, the outputs of the  $V_{dq}$  and  $I_{dq}$  are fed as inputs to Fig. 2b. The parameters  $C_1$ ,  $C_2$  and the  $PI$  controllers coefficients together with the upper and lower bounds of the saturation blocks in Fig. 2b are all defined in Section 6. The outputs of the Fig. 2b, regarded as the imaginary and real values of a complex number, are the inputs of the Fig. 2c. These inputs are converted to the amplitude and phase angle of the same complex value. The amplitude and the phase signals, together with the voltage angle  $\omega t$ , obtained from the PLL in the Fig. 2a, constitute the three phase signal fed to the PWM in Fig. 2c. Finally, each PWM sends the switching signals to the three level inverter of its corresponding DG which is illustrated in Fig. 3.

## 6 Simulations

In this section, the performance of the proposed control methods explained in Section 4.4 is evaluated through the simulation of a microgrid consisting of six inverter-based DGs shown in Fig. 4. The model layout in Fig. 4 is inspired from Matlab-based example available in [35] and the studies in [32, 34]. Then, the performances of the strategies 1 and 3, provided in (25) and (14) respectively, are juxtaposed with the performance of the controller in Section 4.4. The simulations are accomplished using the Simscape toolbox of Matlab. The simulated DGs are numbered from 1 to 6 and are connected to the main grid in parallel as depicted in Fig. 4. Each DG has a corresponding agent in the cyber layer where the updated value of the desired output power is computed by the agents using the information obtained through their bidirectional communication structure, as shown in Fig. 5. Note that the communication graph of the DGs in Fig. 5 is connected per its definition in Section 2.



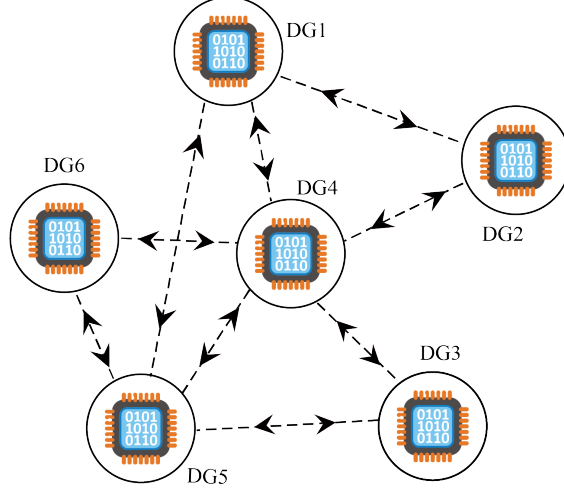


Figure 5: Communication graph of the simulated DGs

As the communication graph in Fig. 5 is a bidirectional graph, per Section 2, the adjacency matrix of the graph is symmetric. The adjacency and degree matrices are chosen as

$$A = \begin{bmatrix} 0 & 6 & 0 & 6 & 6 & 0 \\ 6 & 0 & 0 & 6 & 0 & 0 \\ 0 & 0 & 0 & 6 & 6 & 0 \\ 6 & 6 & 6 & 0 & 6 & 6 \\ 6 & 0 & 6 & 6 & 0 & 6 \\ 0 & 0 & 0 & 6 & 6 & 0 \end{bmatrix}, D = \begin{bmatrix} 18 & 0 & 0 & 0 & 0 & 0 \\ 0 & 12 & 0 & 0 & 0 & 0 \\ 0 & 0 & 12 & 0 & 0 & 0 \\ 0 & 0 & 0 & 30 & 0 & 0 \\ 0 & 0 & 0 & 0 & 24 & 0 \\ 0 & 0 & 0 & 0 & 0 & 12 \end{bmatrix} \quad (53)$$

From Section 2, the correlated Laplacian matrix  $L = A - D$  is defined as

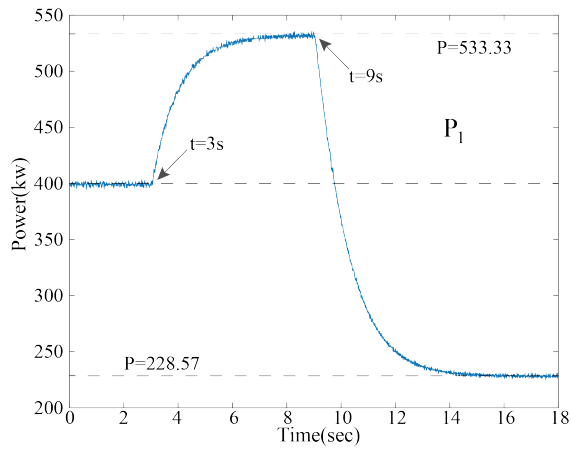
$$L = \begin{bmatrix} 18 & -6 & 0 & -6 & -6 & 0 \\ -6 & 12 & 0 & -6 & 0 & 0 \\ 0 & 0 & 12 & -6 & -6 & 0 \\ -6 & -6 & -6 & 30 & -6 & -6 \\ -6 & 0 & -6 & -6 & 24 & -6 \\ 0 & 0 & 0 & -6 & -6 & 12 \end{bmatrix} \quad (54)$$

For the simulations, we set  $h = 10$  in (7), (38b) and (52). Let the maximum capacity of the DGs  $P_{i,max}$  for  $i = 1, 2, \dots, 6$  be

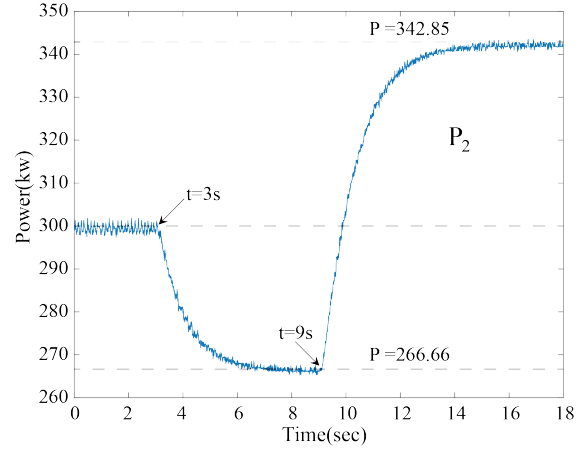
$$\begin{aligned} P_{1,max} &= 600 \text{ kW} & P_{2,max} &= 450 \text{ kW} & P_{3,max} &= 300 \text{ kW} \\ P_{4,max} &= 150 \text{ kW} & P_{5,max} &= 750 \text{ kW} & P_{6,max} &= 150 \text{ kW} \end{aligned} \quad (55)$$

Thus, the maximum capacity of the whole microgrid is  $P_T = \sum_{i=1}^6 P_{i,max} = 2400 \text{ kW}$ , and assume the load demand is  $P_L = 1600 \text{ kW}$ . According to Section 3, the agents have knowledge of  $P_L$  at all times and  $P_T$  at initial time. Therefore, each agent is able to compute the proportional power share ratio  $r = \frac{P_L}{P_T}$  defined in (5), independently, which is  $\frac{2}{3}$ , initially. Therefore, the output power of each  $DG_i$  for  $i = 1, 2, \dots, 6$ , based on the proportional power sharing, must be,

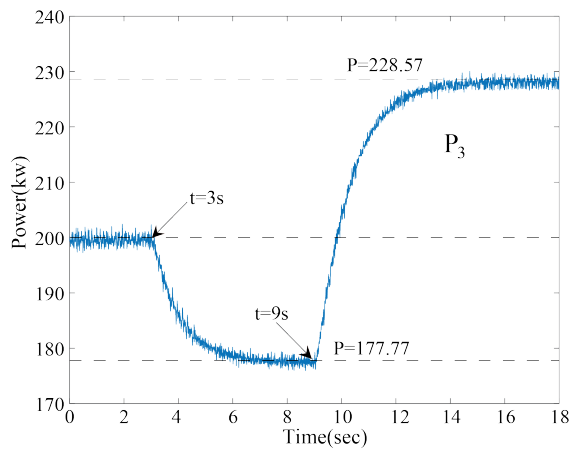
$$\begin{aligned} P_1 &= 400 \text{ kW} & P_2 &= 300 \text{ kW} & P_3 &= 200 \text{ kW} \\ P_4 &= 100 \text{ kW} & P_5 &= 500 \text{ kW} & P_6 &= 100 \text{ kW} \end{aligned} \quad (56)$$



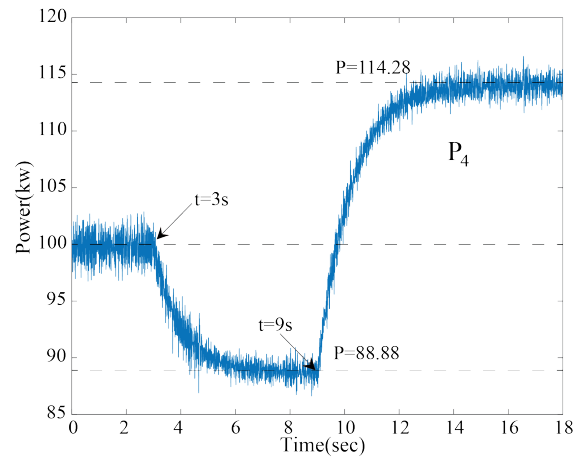
(a)



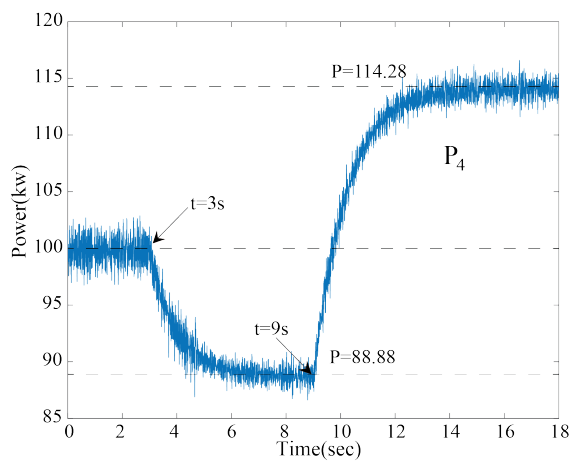
(b)



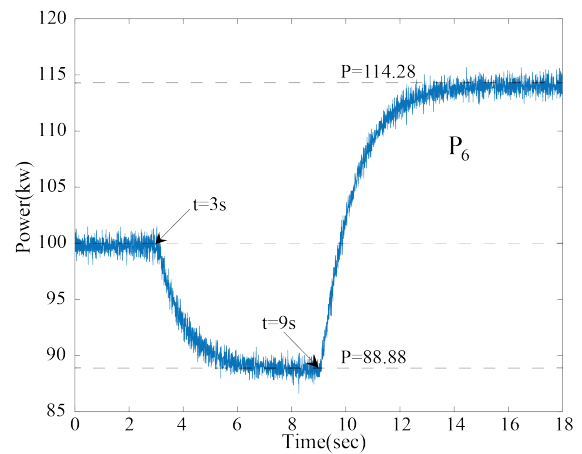
(c)



(d)



(e)



(f)

Figure 6: Output powers  $P_i$ ,  $i = 1, 2, \dots, 6$ , under a variation in  $P_{1,max}$  are depicted in the figures a, b, c, d, e and f, respectively.

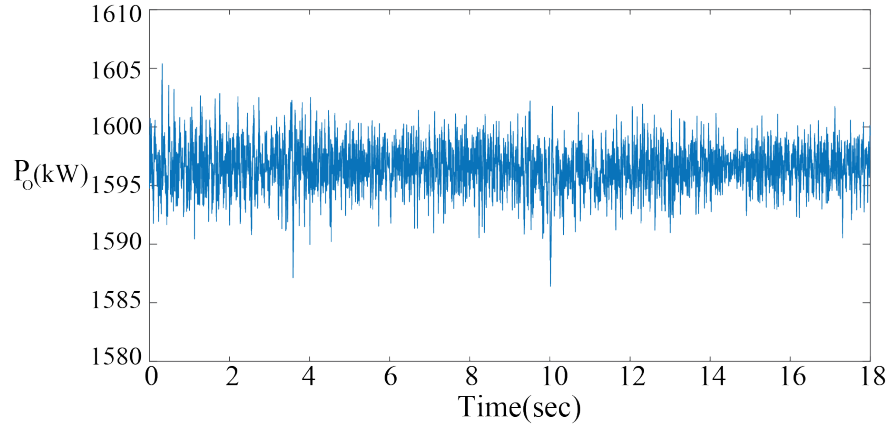


Figure 7: Microgrid total output power  $P_O$  obtained from the proposed control method of Section 4.4

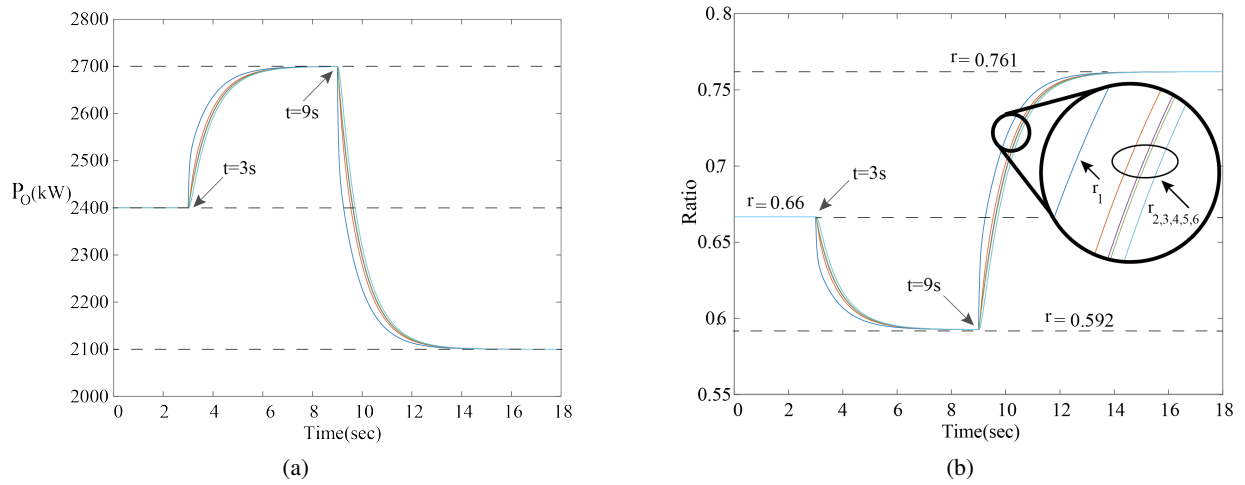


Figure 8: Consensus trajectories of agents on  $\tilde{P}_T$  from (38b) and trajectories of  $r_i$ ,  $i = 1, 2, \dots, 6$ , from (34). (a) Consensus trajectories on  $\tilde{P}_T$  (b) The signals  $r_i$

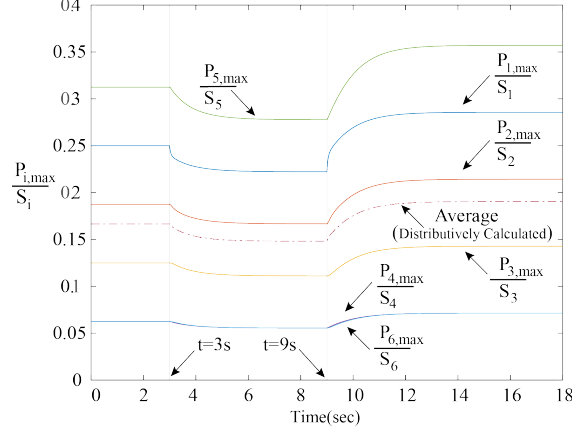


Figure 9: Individual  $P_{i,max}/s_i(t)$  and the average  $P_{i,max}/s_i(t)$  at each time step, as defined in (42) and (43)

During  $t = [0, 3]sec$ , the power capacity of each DG remains unchanged and hence, each of the DGs generates its active power share as calculated in (56). At  $t = 3sec$  the power capacity of DG<sub>1</sub> undergoes a step change, thereby  $P_T$  has an increment of  $300kW$ , and at  $t = 9sec$  we introduce a decrement of  $600kW$  to the capacity of DG<sub>1</sub>.

The simulated microgrid consists of several components such as inverters, output filters of inverters, transformers, PWM, PI controllers, line impedance, loads, DC resources, measurement units, PLL and abc/dq0 converters. To emulate the main grid a dispatchable generator is considered in the simulation as shown in Fig. 4. The parameters of the transformer that connects the main grid to the distribution system and those of the transformers which connect the DGs to the distribution system are given in Table 1. The parameters of the distribution system are provided in Table 2. The PI controllers depicted in Fig. 2b are identical. The PI controllers of all DGs are also identical, meaning they all have the same  $P$  and  $I$  gains, chosen as  $k_p = 0.3$  and  $k_I = 30$ , respectively.

The energy resource of each DG is simulated as a DC power source, then by utilizing an inverter, the DC current converts to the AC current, as shown in Fig. 3. In the same figure, to remove the harmonics from the output power of the inverter, an output filter is applied and then connected to the main grid via a transformer, as illustrated in Fig. 3. The output filter consists of RL and RC branches. The resistive and inductive elements of each RL component are set as  $R_1 = 5.4946 \times 10^{-4}\Omega$  and  $L = 1.4575 \times 10^{-4}H$ , respectively. The RC components for the output filters of each individual DG<sub>*i*</sub> arranged in the delta format have  $P_i(W)$  and reactive power  $Q_i(kVar)$  as given in Table 3. In Fig. 2b,  $C_1 = 0.0039$ ,  $C_2 = 0.21$ , and the upper and lower limit of the saturation blocks are  $+1.5$  and  $-1.5$ , respectively. The power control of each DG established in the physical layer is depicted in Fig. 2.

Starting from  $t = 3sec$ ,  $P_{1,max}$  increases from  $600kW$  to  $900kW$ . Therefore, the microgrid maximum power capacity increases from  $2400kW$  to  $2700kW$ . Based on the approach explained in Section 4.4, the finite-time algorithm in (45)-(49) is embedded in the consensus algorithm (38b) to have DGs apply the proposed control law in (34) and (38), distributively. The results of the simulations are shown in Fig. 6 where  $P_1$  increases and  $P_i$ ,  $i = 2, 3, 4, 5, 6$ , decreases. During  $t = [3, 9]sec$ , the microgrid output power  $P_O$  remains almost equal to  $P_L = 1600kW$ , as shown in Fig. 7. The slight difference between  $P_O$  and  $P_L$  is due to resistive losses in the DGs due to the resistor elements shown in Fig. 3. Considering (38b), the six estimation variables  $s_i$  for all  $i = 1, 2, \dots, 6$  are updated through the information exchange until they reach a consensus concerning  $\hat{P}_T = 2700kW$  as demonstrated in Fig. 8a. The ratios of  $r_i = \frac{P_L}{s_{i,max}}$ , for  $i = 1, 2, \dots, 6$ , are shown in Fig. 8b, where before reaching a consensus during  $t = (3, 8)sec$ , these ratios are different, however they become almost identical during  $t = [8, 9]sec$ . Figure 6 illustrates that after the

Table 1: Parameters of the Transformers

Transformer Connected to DGs			Transformer Connected to Dispatchable Generator		
Parameter		Value	Parameter		Value
Nominal Power (kVA)		100	Nominal Power (kVA)		47000
Nominal Frequency (Hz)		60	Nominal Frequency (Hz)		60
winding 1	$V_{1,rms,ph-ph,kV}$	25	winding 1	$V_{1,rms,ph-ph,kV}$	1200
	$R_1(pu)$	0.0012		$R_1(pu)$	0.0026
	$L_1(pu)$	0.03		$L_1(pu)$	0.08
winding 2	$V_{1,rms,ph-ph,V}$	270	winding 2	$V_{2,rms,ph-ph,kV}$	25
	$R_2(pu)$	0.0012		$R_2(pu)$	0.0026
	$L_2(pu)$	0.03		$L_2(pu)$	0.08
Magnetization resistance Rm (pu)		200	Magnetization Resistance Rm (pu)		500
Magnetization inductance Lm (pu)		200	Magnetization Inductance Lm (pu)		500

Table 2: Parameters of the Grid

Parameter		Value
Load 1 Nominal Voltage ( $kV_{ph-ph}$ )		25
Load 1 Active Power P (kW)		250
Load 2 Active Power P (kW)		2000
Load 3 Power S (kVA)		30000+j2000
Line 1 $Z_1$ Positive and Zero Sequence	Length (km)	8
	$R(\Omega/km)$	[0.1153 0.413]
	$L(H/km)$	[1.05e-3 3.32e-3]
	$C(F/km)$	[11.33e-009 5.01e-009]
Line 2 $Z_2$ Positive and Zero Sequence	Length (km)	14
	$R(\Omega/km)$	[0.1153 0.413]
	$L(H/km)$	[1.05e-3 3.32e-3]
	$C(F/km)$	[11.33e-009 5.01e-009]
Nominal Frequency (Hz)		60

Table 3: Active and reactive powers of RC components of each output filter

DG Number	Active Power(W)	Reactive Power(kVar)
1	400	20
2	200	10
3	600	30
4	500	25
5	300	15
6	400	20

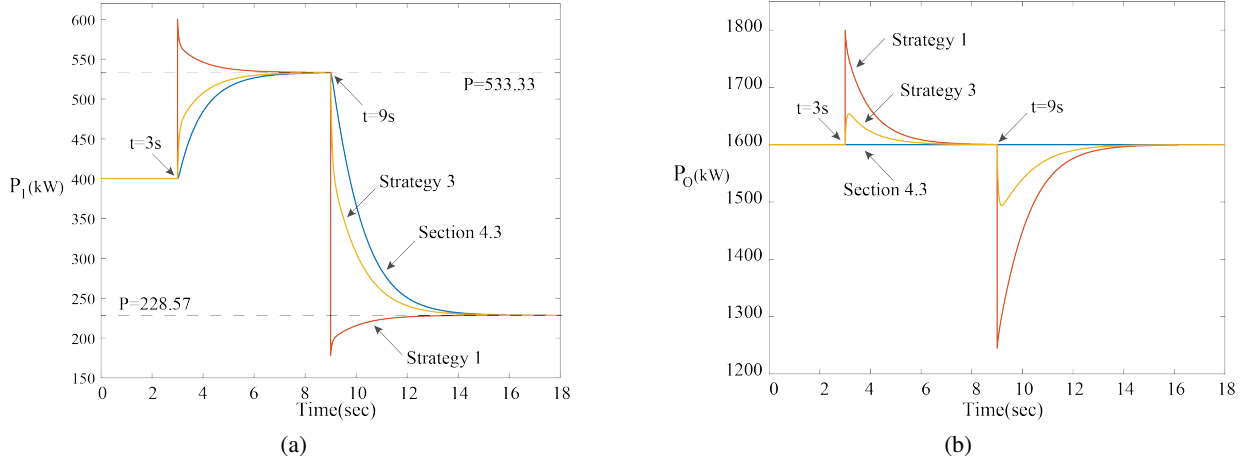


Figure 10: (a) Output power  $P_1$  according to Strategies 1, 3 and the proposed controller of Section 4.4 and (b) Their corresponding microgrid total power  $P_O$

consensus algorithm converges, the steady state values of the output powers of DGs are  $P_1 = 533.33kW$ ,  $P_2 = 266.66kW$ ,  $P_3 = 177.77kW$ ,  $P_4 = 88.88kW$ ,  $P_5 = 444.44kW$  and  $P_6 = 88.88kW$ . Recalling the finite-time average consensus algorithm is embedded in the consensus algorithm, at each time step of evolution of consensus algorithm, the finite-time algorithm is applied. Through this approach, the agents compute the average of  $\frac{P_{i,max}}{s_i(t)}$  for  $i = 1, 2, \dots, 6$  in a distributed way where its corresponding result is illustrated in Fig. 9.

The next variation of the microgrid maximum power capacity occurs at  $t = 9s$  where  $P_{1,max}$  decreases for  $-600kW$ . Therefore, starting from  $t = 9sec$ , the current capacity of the microgrid which is  $P_T = 2700kW$  changes to  $\tilde{P}_T = 2100kW$ . Then, similar to the same procedure adopted in reaction to a change in a microgrid capacity, the control method in (34) and (38) is triggered. Hence, during  $t = [9, 18]sec$ , according to Fig. 8a, the agents have reached to another consensus on the maximum power capacity of the microgrid which is  $2100kW$ . Figure 6a demonstrates that  $P_1$  becomes  $228.57kW$  after the convergence during  $[9, 18]sec$ . Figure 6 also shows that the output power of the other DGs have increased due to the microgrid capacity reduction. The power sharing ratio  $r_i$  for  $i = 1, 2, \dots, 6$  are shown in Fig. 8b. The figure illustrates that, during the transient duration of  $(9, 15)sec$ ,  $r_i$  ratios are not equal. On the contrary, they converge to steady state conditions in  $[14, 18]sec$ . Furthermore, from Fig. 7,  $P_O$  remains practically equal to  $P_L = 1600kW$ . In Fig. 10a, the results of the proposed control algorithm in Section 4.4 is compared with the results of the strategies defined as (14) and (25) in Section 4.3. From this figure, it is clear that the output power of  $P_1$  obtained from the proposed control algorithm Section 4.4 differs from the other two ones during the transient duration. However, after the transient durations of  $(3, 8)sec$  and  $(9, 15)sec$  the output power of  $P_1$  from all three methods are the same. Figure 10b demonstrates that the approaches of (14) and (25) are ineffective to address the load demand. They produce significant deviation in  $P_O$  from  $P_L$  during transient. On the other hand, upon applying the method of Section 4.4, the deviation drastically reduces, both for increase and decrease in maximum power capacity of  $DG_1$ .

## 7 Conclusion

In this research, the problem of distributed proportional power sharing is studied for microgrids that operate in the grid-connected mode. Firstly, a consensus algorithm is designed through which, under a variation in the maximum power capacity of a DG, all DGs in the microgrid estimate the updated microgrid capacity. Utilizing the estimations, they generate their output powers in a distributed manner. Stability and convergence of the consensus algorithm are proven. While the consensus algorithm operates in the cyber layer,

power commands are sent to the DGs at the physical layer using multiple strategies, discussed in the research. In this regards, practical issues such as ensuring power commands are within acceptable bounds during the transient time of the consensus method, are addressed. However, the consensus algorithm along with the aforementioned strategies does not guarantee maintaining load power during the transient time. Therefore, a modified strategy is proposed to guarantee a match between demanded and delivered power during transient, while the DGs reach a new consensus following a perturbation in grid capacity. The distributed controller is tested in a simulated microgrid. The microgrid is modeled in Matlab/Simulink using the Simscape toolbox. A complete description of the model along with parameters values used for simulation, are given. Simulation results confirm the effectiveness of the proposed strategy.

## Appendix

### Proof of Lemma 3

*Proof.* From (13), we note that  $y_i = s_i - \tilde{P}_T$ . Since Lemma 1 shows that  $-(L + \Delta)$  is Hurwitz, therefore from (13) we have,

$$y(t) = e^{-(L+\Delta)t}y(t_0) \Rightarrow \|y(t)\| \leq \|e^{-(L+\Delta)t}\| \|y(t_0)\| \quad (57)$$

As explained in Lemma 1,  $-(L + \Delta)$  is diagonalizable and all of its eigenvalues are negative and real. Assuming  $\lambda_1 < 0$  is the largest eigenvalue of  $-(L + \Delta)$  and since  $y(t_0) = -\delta \mathbf{1}$ , we have,

$$\|y(t)\| \leq e^{\lambda_1 t} \|y(t_0)\| = e^{\lambda_1 t} \sqrt{N} |\delta| \leq \sqrt{N} |\delta| \quad (58)$$

Hence,  $\|y\|$  is bounded. Since  $|y_i| \leq \|y(t)\|$ , therefore

$$|y_i(t)| \leq \sqrt{N} |\delta| \quad \forall i = 1, 2, \dots, N \quad (59)$$

If  $|\delta| < \theta P_T / (1 + \sqrt{N})$ , then it follows that

$$|y_i(t)| \leq \sqrt{N} |\delta| \leq \sqrt{N} \theta P_T / (1 + \sqrt{N}) \quad (60)$$

and since  $y_i = s_i - \tilde{P}_T$ , therefore we have

$$\begin{aligned} \tilde{P}_T - \sqrt{N} \theta P_T / (1 + \sqrt{N}) &\leq s_i(t) \leq \\ \tilde{P}_T + \sqrt{N} \theta P_T / (1 + \sqrt{N}) & \end{aligned} \quad (61)$$

Since  $\tilde{P}_T = P_T + \delta$ , and from the assumption  $|\delta| < \theta P / (1 + \sqrt{N})$ , we have

$$\begin{aligned} P_T - \theta P_T / (1 + \sqrt{N}) - \sqrt{N} \theta P_T / (1 + \sqrt{N}) &\leq s_i(t) \\ &\leq P_T + \theta P_T / (1 + \sqrt{N}) + \sqrt{N} \theta P_T / (1 + \sqrt{N}) \end{aligned} \quad (62)$$

Thus,

$$(1 - \theta) P_T \leq s_i(t) \leq (1 + \theta) P_T \quad (63)$$

Since for all  $t > t_0$ , the output power of each DG<sub>*i*</sub> should satisfy  $P_i(t) = \frac{P_L}{s_i(t)} P_{i,max} < P_{i,max}$ , it is required that  $s_i(t) > P_L$  for all  $t > t_0$ . For guaranteeing  $s_i(t) > P_L$ , from (63), we can impose  $(1 - \theta) P_T > P_L$ . Therefore, under the dynamics of  $\mathbf{S}$  in (7),  $P_T > P_L / (1 - \theta)$  or  $1 - (P_L / P_T) > \theta$  ensures that  $P_i(t) < P_{i,max}$ . This completes the proof.  $\square$

**Observation on  $\delta$ :** Lemma 3 gives the condition  $|\delta| < \theta P_T / (1 + \sqrt{N})$  to prevent unfavorable transients in  $s_i(t)$ . To demonstrate that this condition is not restrictive as  $N$  increases, we consider a change in  $N$  to  $N + 1$  and a corresponding change from  $P_T$  to  $P_T + P_{N+1,max}$ . Further, we impose

$$\frac{\theta(P_T + P_{N+1,max})}{1 + \sqrt{N+1}} > \frac{\theta P_T}{1 + \sqrt{N}} \quad (64)$$

to derive the condition under which  $|\delta|$  will increase as we increase  $N$  to  $N + 1$ . From (64), we have,

$$P_{N+1,max} > \left[ \frac{\sqrt{N+1} - \sqrt{N}}{1 + \sqrt{N}} \right] P_T \quad (65)$$

From (65), it can be observed that  $P_{N+1,max}$  can be only a small fraction of  $P_T$  to allow  $|\delta|$  to increase rather than decrease. For instance, if  $N = 3$ , then  $P_{N+1,max} > 0.098P_T$ , and if  $N = 8$ , then  $P_{N+1,max} > 0.045P_T$  which are small fractions of  $P_T$ . In addition, comparing the right hand side of (65) with the average of  $P_T$ ,  $P_{T,avg} = P_T/N$ , we obtain the minimum ratio of  $P_{N+1,max}/P_{T,avg}$  as following

$$N \left[ \frac{\sqrt{N+1} - \sqrt{N}}{1 + \sqrt{N}} \right] \quad (66)$$

Equation (66) is strictly less than  $\frac{1}{2}$  and it converges to  $\frac{1}{2}$  for large values of  $N$ . This proves that  $P_{N+1,max}$  is required to be  $P_{N+1,max} \geq (1/2)P_{avg}$  at the worst cases to satisfy the condition on  $|\delta|$ . Therefore, the condition on  $|\delta|$  is not restrictive.

## References

- [1] J. Rocabert, A. Luna, F. Blaabjerg, and P. Rodriguez, "Control of power converters in ac microgrids," *IEEE transactions on power electronics*, vol. 27, no. 11, pp. 4734–4749, 2012.
- [2] J. He, Y. Pan, B. Liang, and C. Wang, "A simple decentralized islanding microgrid power sharing method without using droop control," *IEEE Transactions on Smart Grid*, vol. 9, no. 6, pp. 6128–6139, 2017.
- [3] Y. Du, X. Lu, J. Wang, and S. Lukic, "Distributed secondary control strategy for microgrid operation with dynamic boundaries," *IEEE Transactions on Smart Grid*, 2018.
- [4] Y. Zhang, H. J. Jia, and L. Guo, "Energy management strategy of islanded microgrid based on power flow control," in *2012 IEEE PES Innovative Smart Grid Technologies (ISGT)*, pp. 1–8, IEEE, 2012.
- [5] Y. Han, H. Li, P. Shen, E. A. A. Coelho, and J. M. Guerrero, "Review of active and reactive power sharing strategies in hierarchical controlled microgrids," *IEEE Transactions on Power Electronics*, vol. 32, no. 3, pp. 2427–2451, 2017.
- [6] E. Barklund, N. Pogaku, M. Prodanovic, C. Hernandez-Aramburo, and T. C. Green, "Energy management in autonomous microgrid using stability-constrained droop control of inverters," *IEEE Transactions on Power Electronics*, vol. 23, no. 5, pp. 2346–2352, 2008.
- [7] Y. Deng, Y. Tao, G. Chen, G. Li, and X. He, "Enhanced power flow control for grid-connected droop-controlled inverters with improved stability," *IEEE Transactions on Industrial Electronics*, vol. 64, no. 7, pp. 5919–5929, 2016.



- [8] Y. Gui, C. Kim, C. C. Chung, J. M. Guerrero, Y. Guan, and J. C. Vasquez, "Improved direct power control for grid-connected voltage source converters," *IEEE Transactions on Industrial Electronics*, vol. 65, no. 10, pp. 8041–8051, 2018.
- [9] Y. Fan, G. Hu, and M. Egerstedt, "Distributed reactive power sharing control for microgrids with event-triggered communication," *IEEE Transactions on Control Systems Technology*, vol. 25, no. 1, pp. 118–128, 2016.
- [10] D. He, D. Shi, and R. Sharma, "Consensus-based distributed cooperative control for microgrid voltage regulation and reactive power sharing," in *IEEE PES Innovative Smart Grid Technologies, Europe*, pp. 1–6, IEEE, 2014.
- [11] M. Mahmud, M. Hossain, H. Pota, and A. Oo, "Robust nonlinear distributed controller design for active and reactive power sharing in islanded microgrids," *IEEE Transactions on Energy Conversion*, vol. 29, no. 4, pp. 893–903, 2014.
- [12] J. M. Guerrero, L. G. De Vicuna, J. Matas, M. Castilla, and J. Miret, "Output impedance design of parallel-connected ups inverters with wireless load-sharing control," *IEEE Transactions on industrial electronics*, vol. 52, no. 4, pp. 1126–1135, 2005.
- [13] J. M. Guerrero, J. Matas, L. G. de Vicuna, M. Castilla, and J. Miret, "Decentralized control for parallel operation of distributed generation inverters using resistive output impedance," *IEEE Transactions on industrial electronics*, vol. 54, no. 2, pp. 994–1004, 2007.
- [14] F. Aalipour and T. Das, "Proportional power sharing consensus in distributed generators," in *ASME 2018 Dynamic Systems and Control Conference*, pp. V002T17A002–V002T17A002, American Society of Mechanical Engineers, 2018.
- [15] G. Chen, F. L. Lewis, E. N. Feng, and Y. Song, "Distributed optimal active power control of multiple generation systems," *IEEE Transactions on Industrial Electronics*, vol. 62, no. 11, pp. 7079–7090, 2015.
- [16] Q.-C. Zhong, "Robust droop controller for accurate proportional load sharing among inverters operated in parallel," *IEEE Transactions on Industrial Electronics*, vol. 60, no. 4, pp. 1281–1290, 2011.
- [17] A. Pantoja and N. Quijano, "A population dynamics approach for the dispatch of distributed generators," *IEEE Transactions on Industrial Electronics*, vol. 58, no. 10, pp. 4559–4567, 2011.
- [18] C.-E. Lin and G. Viviani, "Hierarchical economic dispatch for piecewise quadratic cost functions," *IEEE transactions on power apparatus and systems*, no. 6, pp. 1170–1175, 1984.
- [19] S. Kar and G. Hug, "Distributed robust economic dispatch in power systems: A consensus+ innovations approach," in *2012 IEEE Power and Energy Society General Meeting*, pp. 1–8, IEEE, 2012.
- [20] G. Lou, W. Gu, Y. Xu, M. Cheng, and W. Liu, "Distributed mpc-based secondary voltage control scheme for autonomous droop-controlled microgrids," *IEEE transactions on sustainable energy*, vol. 8, no. 2, pp. 792–804, 2016.
- [21] A. Vaccaro, G. Velotto, and A. F. Zobaa, "A decentralized and cooperative architecture for optimal voltage regulation in smart grids," *IEEE Transactions on Industrial Electronics*, vol. 58, no. 10, pp. 4593–4602, 2011.

- [22] W. Liu, W. Gu, J. Wang, W. Yu, and X. Xi, “Game theoretic non-cooperative distributed coordination control for multi-microgrids,” *IEEE Transactions on Smart Grid*, vol. 9, no. 6, pp. 6986–6997, 2018.
- [23] B. Chaudhuri, R. Majumder, and B. C. Pal, “Wide-area measurement-based stabilizing control of power system considering signal transmission delay,” *IEEE Transactions on Power Systems*, vol. 19, no. 4, pp. 1971–1979, 2004.
- [24] H. Wu, K. S. Tsakalis, and G. T. Heydt, “Evaluation of time delay effects to wide-area power system stabilizer design,” *IEEE Transactions on Power Systems*, vol. 19, no. 4, pp. 1935–1941, 2004.
- [25] L. Xiao and S. Boyd, “Fast linear iterations for distributed averaging,” *Systems & Control Letters*, vol. 53, no. 1, pp. 65–78, 2004.
- [26] F. Dörfler, J. W. Simpson-Porco, and F. Bullo, “Electrical networks and algebraic graph theory: Models, properties, and applications,” *Proceedings of the IEEE*, vol. 106, no. 5, pp. 977–1005, 2018.
- [27] T. Charalambous, Y. Yuan, T. Yang, W. Pan, C. N. Hadjicostis, and M. Johansson, “Distributed finite-time average consensus in digraphs in the presence of time delays,” *IEEE Transactions on Control of Network Systems*, vol. 2, no. 4, pp. 370–381, 2015.
- [28] H. K. Khalil, *Nonlinear systems*, vol. 3. Prentice hall Upper Saddle River, NJ, 2002.
- [29] M. Mesbahi and M. Egerstedt, *Graph theoretic methods in multiagent networks*. Princeton University Press, 2010.
- [30] R. A. Horn and C. R. Johnson, *Matrix analysis*, vol. 2. Cambridge University Press, 2013.
- [31] F. Aalipour, A. Gusrialdi, and Z. Qu, “Distributed optimal output feedback control of heterogeneous multi-agent systems under a directed graph,” *IFAC-PapersOnLine*, vol. 50, no. 1, pp. 5097–5102, 2017.
- [32] J. Schiffer, T. Seel, J. Raisch, and T. Sezi, “Voltage stability and reactive power sharing in inverter-based microgrids with consensus-based distributed voltage control,” *IEEE Transactions on Control Systems Technology*, vol. 24, no. 1, pp. 96–109, 2015.
- [33] H. Cai and G. Hu, “Distributed robust hierarchical power sharing control of grid-connected spatially concentrated ac microgrid,” *IEEE Transactions on Control Systems Technology*, vol. 27, no. 3, pp. 1012–1022, 2018.
- [34] V. Nasirian, Q. Shafiee, J. M. Guerrero, F. L. Lewis, and A. Davoudi, “Droop-free distributed control for ac microgrids,” *IEEE Transactions on Power Electronics*, vol. 31, no. 2, pp. 1600–1617, 2016.
- [35] “250-kw grid-connected pv array.” <https://www.mathworks.com/help/physmod/sps/examples/250-kw-grid-connected-pv-array.html>.